POAC'25
St. John's, Newfoundland and Labrador, Canada

Proceedings of the 28th International Conference on Port and Ocean Engineering under Arctic Conditions
Jul 13-17, 2025
St. John's, Newfoundland and Labrador
Canada

Parameter-Based Generator for Ice Floe Fields

Lina Sapp[1,2], Franz von Bock und Polach[1]
[1] Institute for Ship Structural Design (M-10), Hamburg University of Technology (TUHH), Hamburg, Germany
[2] Department of Civil and Environmental Engineering (IBM), Norwegian University of Science and Technology (NTNU), Trondheim, Norway

ABSTRACT
With decreasing ice thickness and ice extension in summer, shipping in and close to ice-covered areas and the marginal ice zone are of raising interest. To determine the exact forces due to the icebreaking and to enable a more precise and less over dimensioned design of ice-going vessels, models can be a helpful tool. To use these models to simulate the icebreaking process, the ice has to be modelled as well. This work presents a new randomized approach for the generation of ice floe fields based on common simple ice observation parameters and reflecting the real ice floe arrangement: The ice floe field is modified by constrained optimization after the ice floes are placed randomly. The generated ice floe fields are evaluated for different parameter sets, to determine the influence and sensitivity of the different ice observation parameters. The filling of the parameter space depending on the number of generated floe fields per parameter set is estimated. Furthermore, suggestions on how to use these floe fields are given.

KEY WORDS: Ice field generation; Ice floe arrangement; Monte Carlo simulation; Ice coverage

INTRODUCTION
While shipping in ice-covered areas is continuously a topic of high interest, especially with decreasing ice thickness in summer, the exact forces due to the icebreaking process still requires further attention. In order to enable a more precise and less over dimensioned design of ice-going vessels, models are used. To apply these models on full-scale data, the ice conditions have to be monitored and prepared for being an input value to the simulation tools. For most of the test scenarios, the ice conditions are only available as egg code or extended observations based on the egg code for relatively large regions.
In the past, some approaches have been conducted to generate ice floe fields. Løset (1994) modelled a floe field by circular plates ordered in a full rectangular grid. Sun and Shen (2012) also placed the ice floes in a regular grid. In both cases, the floe fields can change during the simulation time dynamically, but the initial conditions are the same for all simulation runs.
To generate more natural floe fields without repeating patterns in the floe constellation, Huang et al. (2022) developed two methods for the floe field generation. For floe fields with lower ice concentration ($\leq 70\,\%$), they introduced a sequential generator that places one floe per step and checks the condition of no overlapping of floes. Especially with higher ice concentrations, this generator might end in a dead end, if not sufficient space for floe placing is left. For higher

ice concentrations, they presented the genetic generator, which is able to place floes in a field with a higher ice concentration at the price of higher computational costs. Both generators take the concentration and size distribution as input parameters. Another approach for the floe field generation is the application of Voronoi diagrams as shown by Hopkins et al. (2004) and Zhang et al. (2024). This generator creates ice floes with arbitrary shapes, but the size distributions can not be defined by a constant input value due to the random placement of the Voronoi seeds.
The clustering behaviour of ice floes and the conglomeration of smaller floes around larger ones was described by Herman (2012). This phenomenon is ignored by the completely random placement of floes in the existing floe field generators or in small scale experimental setups (Zong et al., 2020).
This work combines the random placement of ice floes with the observed clustering behaviour of ice floes and presents an algorithm that works for arbitrary ice concentrations by placing ice floes and then optimizing the whole floe field instead of single floe positions. Like this, the relation between the floe positions is respected and the missing representation of clustered ice floes can be solved.
Applying a model on full-scale data to compare different ship parameters needs full-scale input data. Neither the egg code nor the extended ice observations contains specific information about the positioning of the ice floes, but only the size, thickness and concentration distributions. To determine the positions for each floe and create a representable floe field based on the observed data, this work presents a method and evaluates its applicability for simulating full-scale tests.

MODEL

In this work, the ice floes are modelled as circular disks as described by Herman (2011). To transform the ice observation data to ice floe fields usable as input to simulations, e.g. icebreaking simulations, the ice distributions are first computed, then all floes are placed randomly and afterwards the whole floe field is optimized regarding no intersections as described in (Sapp, 2023). The ice observation data used in this work are an extended version of the egg code principle and consists of the ice concentration $\bar{c}_{\mathrm{ice}}$, the ice thickness $\bar{h}_{\mathrm{ice}}$ and the diameter distribution $\mathbf{d}_{\%}$ within the floes. The ice concentration and the ice thickness are mean values for the whole observed area. To describe the diameter distributions $\mathbf{d}_{\%}$, the different size categories

$$\mathbf{d}_{\mathrm{ice}} = \{2.5, 7.5, 15\}\ \mathrm{m} \tag{1}$$

are defined. These size categories can be adapted and extended, to fit varying sets of ice conditions.
The number of floes per size category is

$$m_d = d_{\%} m_{\mathrm{floe}} \tag{2}$$

with the total number of floes

$$m_{\mathrm{floe}} = \lceil \frac{A_{\mathrm{ice,tot}}}{\bar{A}_{\mathrm{ice}}} \rceil \tag{3}$$

with the total ice covered area

$$A_{\mathrm{ice,tot}} = \bar{c}_{\mathrm{ice}} A_{\mathrm{field}}, \tag{4}$$

the mean area per floe

$$\bar{A}_{\mathrm{ice}} = \langle \mathbf{a}_{\mathrm{ice,cat}}, \mathbf{d}_{\%} \rangle \tag{5}$$

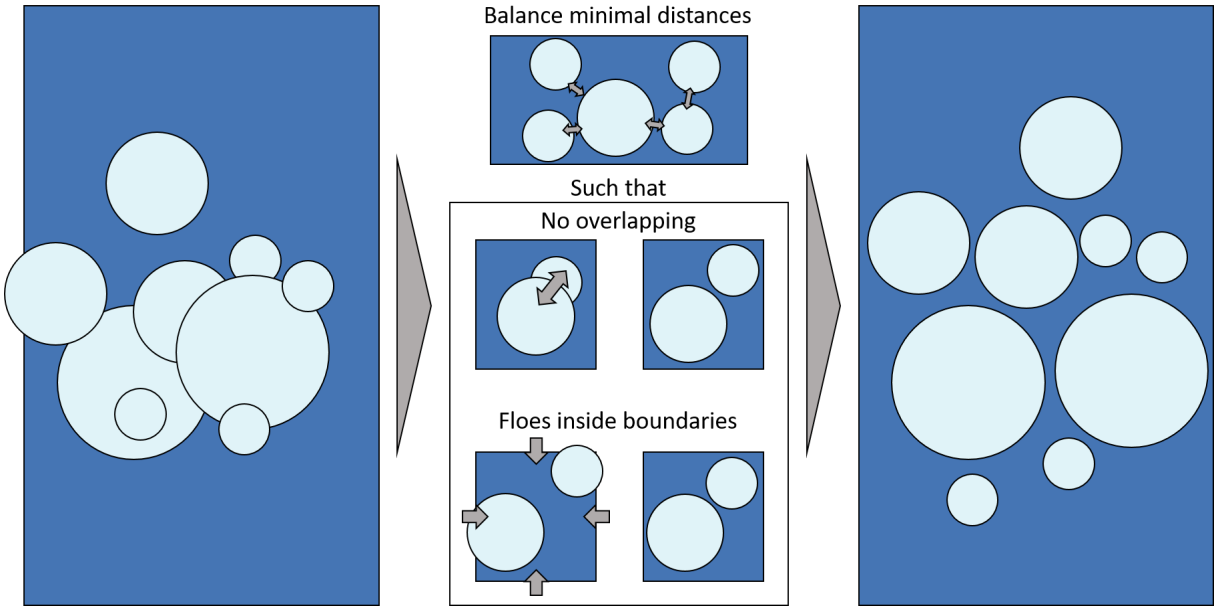

Figure 1: Graphical overview about the optimization problem solving the overlapping-free floe placement.

and the area per size category

$$\mathbf{a}_{\text{ice,cat}} = \pi \frac{\mathbf{d}_{\text{ice}}{}^2}{2}. \tag{6}$$

An example for the diameter distribution is

$$\mathbf{d}_{\%} = \{20, 40, 40\}\ \% \tag{7}$$

as given by the parameter sets A and B in Table 1.
If the number of floes per diameter category m_d is known, the floes are placed randomly in a defined rectangular field of length x_{field} and width y_{field} by setting the centre position of every ice floe i to

$$\mathbf{x}^i_{\text{pos}} = \begin{pmatrix} x_{\text{rand}} x_{\text{field}} \\ y_{\text{rand}} y_{\text{field}} \end{pmatrix}, \quad x_{\text{rand}}, y_{\text{rand}} \in [0, 1]. \tag{8}$$

Every floe is described by a position $\mathbf{x}^i_{\text{pos}}$ and a radius r^i, which leads to the floe vector $(x^i_{\text{pos}}, y^i_{\text{pos}}, r^i)$ for every floe i. If the designated use of the floe fields requires more complex shapes than the circular ones presented, the pose must be described not only by the position $(x^i_{\text{pos}}, x^i_{\text{pos}})$, but also by the orientation and instead of optimizing only the positions, the poses must be optimized.
Afterwards, the floe positions are optimized using a sequential quadratic programming (SQP) algorithm to ensure that no overlapping between ice floes occurs and all floes are still within the boundaries given by x_{field} and y_{field}. This procedure is depicted in Figure 1 and described by the optimization problem

$$\min_{\mathbf{X}_{\text{pos}}} f\left(\mathbf{X}_{\text{pos}}\right) \qquad s.t.\ g_i\left(\mathbf{X}_{\text{pos}}\right) \leq 0,\ i \in \{1, 2, 3, 4, 5\}$$

with the cost function

$$f\left(\mathbf{X}_{\mathrm{pos}}\right)=\left|\min_{\mathbf{x}_{\mathrm{pos}}^{i}}\left(\min_{\mathbf{x}_{\mathrm{pos}}^{j}}\left(d_{\mathbf{x}_{\mathrm{pos}}^{i},\mathbf{x}_{\mathrm{pos}}^{j}}\right)\right)-\max_{\mathbf{x}_{\mathrm{pos}}^{i}}\left(\min_{\mathbf{x}_{\mathrm{pos}}^{j}}\left(d_{\mathbf{x}_{\mathrm{pos}}^{i},\mathbf{x}_{\mathrm{pos}}^{j}}\right)\right)\right|\ \forall i,j\in\{1,2,\ldots,m_{\mathrm{floe}}\}$$

with the Euclidean distances between the floes

$$d_{\mathbf{x}_{\mathrm{pos}}^{i},\mathbf{x}_{\mathrm{pos}}^{j}}=\mathrm{dist}\left(\mathbf{x}_{\mathrm{pos}}^{i},\mathbf{x}_{\mathrm{pos}}^{j}\right)-\left(r_{i}+r_{j}\right).$$

The cost function uses the distance from each floe to its closest neighbour and determines the largest difference between these minimal distances. Minimizing the cost function leads to an equalized distance for every floe to its closest neighbour and therefore amplifies the clustering of ice floes initialized by the random placement.
The constraint of no overlapping of ice floes is described by

$$g_{1}^{ij}\left(\mathbf{X}_{\mathrm{pos}},\mathbf{r}\right)=\begin{cases}-d_{\mathbf{x}_{\mathrm{pos}}^{i},\mathbf{x}_{\mathrm{pos}}^{j}} & i\neq j\\ 0 & i=j\end{cases}$$

which ensures that the pairwise distance between two floes is at least the sum of their radii. To keep all floes within the given field boundaries described by the four corner points $(x_{\min},y_{\min})$, $(x_{\min},y_{\max})$, $(x_{\max},y_{\min})$ and $(x_{\max},y_{\max})$, the following constraints are applied:

$$\begin{aligned}g_{2}\left(\mathbf{X}_{\mathrm{pos}}\right)&=x_{\min}\mathbb{I}_{m_{\mathrm{floe}},1}-\mathbf{X}_{\mathrm{pos}}^{x}\\ g_{3}\left(\mathbf{X}_{\mathrm{pos}}\right)&=\mathbf{X}_{\mathrm{pos}}^{x}-x_{\max}\mathbb{I}_{m_{\mathrm{floe}},1}\\ g_{4}\left(\mathbf{X}_{\mathrm{pos}}\right)&=y_{\min}\mathbb{I}_{m_{\mathrm{floe}},1}-\mathbf{X}_{\mathrm{pos}}^{y}\\ g_{5}\left(\mathbf{X}_{\mathrm{pos}}\right)&=\mathbf{X}_{\mathrm{pos}}^{y}-y_{\max}\mathbb{I}_{m_{\mathrm{floe}},1}\end{aligned}$$

where $\mathbb{I}_{m_{\mathrm{floe}},1}\in\mathbb{R}^{m_{\mathrm{floe}}\times 1}$ describes the vector of ones.

METHOD EVALUATION

Figure 2 shows four exemplary floe fields generated with the same parameter set. Despite the statistical characteristics of all fields being the same, their arrangements vary significantly. This variation is the result of the randomized placement of the ice floes. Determining both, the influence of the parameters as well as a potential convergence of the similarity distribution, is the objective of this section. The first helps to understand the importance of the different observation parameters and especially the sensitivity towards changes. The latter gives a guideline on how many simulations should be run to represent the parameter space of the floe field.
The method presented above is evaluated based on the input sensitivity and precision by a parameter study. Because the ice thickness value is not taken into account for the ice floe placement, it is not regarded in the following study. Therefore, the varied parameters are the average ice concentration $\bar{c}_{\mathrm{ice}}$ and the diameter distribution $\mathbf{d}_{\%}$. The parameter sets used are listed in Table 1. Every parameter set is applied n times. In addition, a convergence study is conducted to estimate the influence of the number of floe fields as well as the convergence of the similarity values.
To quantify the sensitivity and precision, the floe fields have to be compared against each other. A method usually used to assess synthetic data generated for training of neuronal networks is the cosine similarity, which works for large datasets of non-binary vectorized data. The floe

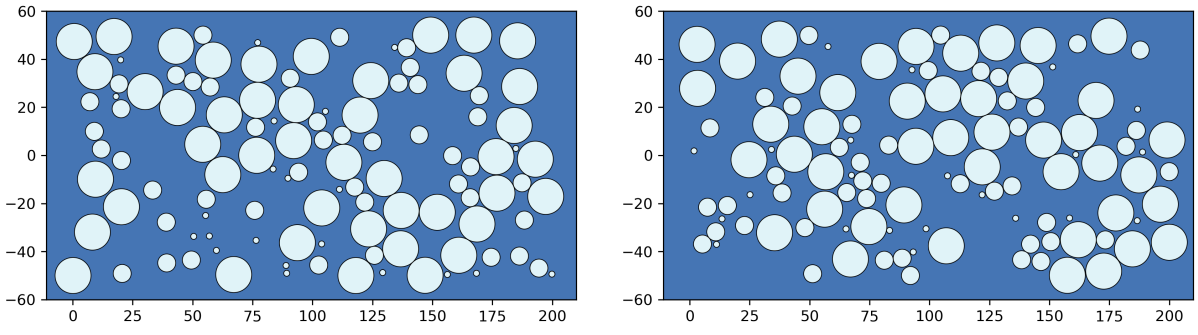

(a) A, 0

(b) A, 1

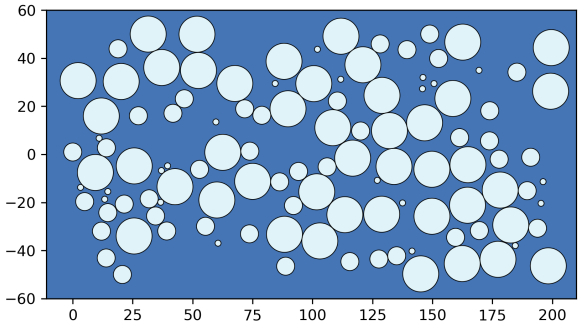

(c) A, 2

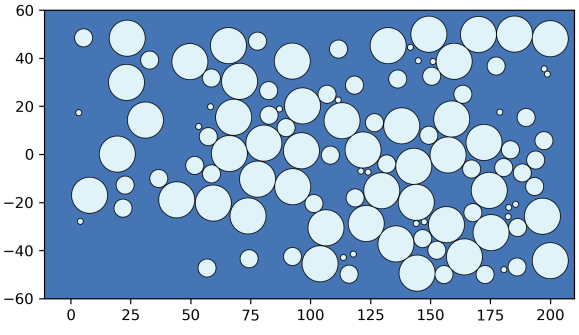

(d) A, 3

Figure 2: Four different examples for a randomized floe field using the data from observation set A as shown in Table 1.

fields generated in this work are also synthetic data in a 2D plane similar to artificial images. Therefore, the cosine similarity is regarded as an appropriate tool to quantify the pairwise similarities between a set of different floe fields.

Similarity quantification

First, the floe field needs to be described: Using a discretization grid of grid size a_{grid} equals the smallest floe diameter ($2.5\,\text{m}$ in this exemplary ice parameter set), the ratio of ice cover is computed per grid cell by

$$c_{\text{ice}}^{xy} = \frac{A_{\text{ice}}^{xy}}{A_{\text{cell}}} \tag{9}$$

with the ice area in the grid cell A_{ice}^{xy} at position (x, y) and the total cell area $A_{\text{cell}} = {a_{\text{grid}}}^2$. Using Equation (9), the ice field with $k \times l$ discretized grid cells can be described by the ice concentration in every grid cell with

$$\mathbf{C}_{\text{ice}} = \begin{pmatrix} c_{\text{ice}}^{11} & c_{\text{ice}}^{21} & \cdots & c_{\text{ice}}^{k1} \\ c_{\text{ice}}^{12} & c_{\text{ice}}^{22} & \cdots & c_{\text{ice}}^{k2} \\ \vdots & \vdots & \ddots & \vdots \\ c_{\text{ice}}^{1l} & c_{\text{ice}}^{2l} & \cdots & c_{\text{ice}}^{kl} \end{pmatrix}. \tag{10}$$

To apply the cosine similarity on these floe field description, the concentration matrix $\mathbf{C}_{\text{ice}}$ needs

to be vectorized by

$$\mathbf{c}_{\text{ice}}^{\text{vec}} = \begin{pmatrix} \mathbf{c}_{\text{ice}}^{1} \\ \mathbf{c}_{\text{ice}}^{2} \\ \vdots \\ \mathbf{c}_{\text{ice}}^{k} \end{pmatrix} \tag{11}$$

with $\mathbf{c}_{\text{ice}}^{i}$ denoting the i-th column of $\mathbf{C}_{\text{ice}}$. The pairwise cosine similarity between n different ice fields of the same parameter set is then calculated by

$$s_{kl} = \frac{\langle \mathbf{c}_{\text{ice},k}^{\text{vec}}, \mathbf{c}_{\text{ice},l}^{\text{vec}} \rangle}{\left|\mathbf{c}_{\text{ice},k}^{\text{vec}}\right| \cdot \left|\mathbf{c}_{\text{ice},l}^{\text{vec}}\right|}, \quad k, l \in \mathbb{N}_0, k, l < n. \tag{12}$$

Table 1: Exemplary ice observation data. The mean ice concentration $\bar{c}_{\text{ice}}$ and the diameter distribution $\mathbf{d}_{\%}$ are varied, whereas the mean ice thickness $\bar{h}_{\text{ice}}$ does not affect the ice distribution and is therefore kept constant.

Key	**Concentration** $\bar{c}_{\text{ice}}$ [%]	**Thickness** $\bar{h}_{\text{ice}}$ [m]	**Diameter Distribution** $\mathbf{d}_{\%}$ [%]		
			$2.5\,\text{m}$	$7.5\,\text{m}$	$15\,\text{m}$
A	50	0.5	20	40	40
B	70	0.5	20	40	40
C	50	0.5	40	30	30
D	70	0.5	40	30	30

Convergence study

To estimate the required number of floe fields to represent the possible floe field configurations described by one parameter set, a convergence study regarding the variance between the floe fields on the same parameter set is conducted. The cosine similarities are computed for varying numbers of floe fields based on the parameter set D from Table 1. The resulting distributions are shown in Figure 3. The standard deviation of the similarity is interpreted as a dimension of the variability of the similarities of the different floe field arrangements. The lower the standard deviation, the lower is the variability of the similarities and therefore the more potential floe field arrangements are represented in the set. The $99\,\%$ confidence interval is used to measure and contextualize the standard deviation and therefore the variability of the different floe field arrangements. It is defined as $[\bar{s} - h, \bar{s} + h]$ with the mean value of all cosine similarities

$$\bar{s} = \frac{2}{n(n+1)} \sum_{k=1}^{n} \sum_{l=k+1}^{n} s_{kl} \tag{13}$$

and the margin of the error

$$h = \text{SE} \cdot t^*. \tag{14}$$

The standard error of the mean is

$$\text{SE} = \frac{\sigma}{\sqrt{\frac{2}{n(n+1)}}} \tag{15}$$

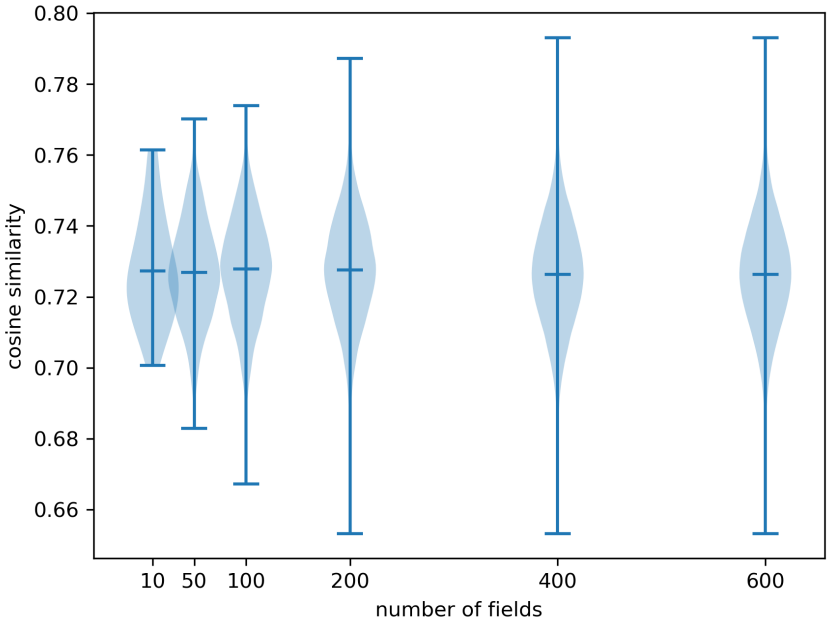

Figure 3: Violin plot of the different cosine similarities for a varying number of generated fields for parameter set D.

with the sample standard deviation

$$\sigma = \sqrt{\frac{2}{n(n+1)} \sum_{k=1}^{n} \sum_{l=k+1}^{n} (s_{kl} - \bar{s})^2} \tag{16}$$

and the critical t-value of the Student's distribution is

$$t^* = t_{\frac{1.99}{2}, n-1}. \tag{17}$$

The confidence intervals are listed in Table 2. For 200 simulated fields, 99% of the cosine similarity values are lying within $\pm 0.075\%$ around the mean value, which correlates with a low standard variation and therefore a high representation of possible floe fields. The spreading can be halved by doubling the number of floe fields. Even though a narrower confidence interval provides a more accurate result, especially when evaluating the floe fields as input in a Monte-Carlo simulation, the relation between computational time and accuracy of the results is expected to be the best between 200 and 400 simulations.

Parameter Study

The floe field generation and the subsequent accuracy estimation is done for different sets of exemplary ice observation data sets as shown in Table 1.

The object of this parameter study is to estimate the influence of the ice concentration and the diameter distribution on the precision. The cosine similarity is interpreted as a value for the precision of the different floe fields. The exact positions of the ice floes in the real scenario are unknown. Hence, no statement about the actual accuracy of the method can me made. Assuming that the ice observation protocol represents the real ice floe field properly, the real floe field is within the range of the synthetic floe fields. This leads to the conclusion that the accuracy is at least as good as the precision and the precision can be taken as an upper bound

Table 2: Confidence intervals $[\bar{s} - h, \bar{s} + h]$ of the cosine similarity for different number of fields. $\bar{s}$ is the mean value of the cosine similarity and $h_{\%} = h/\bar{s}$.

Number of fields	$\bar{s}$	h	$h_{\%}$
10	0.7273	$1.21 \cdot 10^{-2}$	1.664%
50	0.7268	$2.10 \cdot 10^{-3}$	0.289%
100	0.7278	$1.09 \cdot 10^{-3}$	0.150%
200	0.7275	$5.47 \cdot 10^{-4}$	0.075%
400	0.7263	$2.79 \cdot 10^{-4}$	0.038%
600	0.7263	$1.85 \cdot 10^{-4}$	0.025%

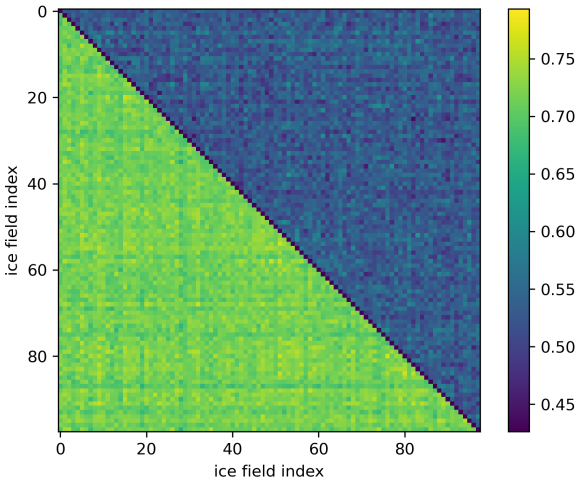

(a) upper right: A, $\bar{s} = 52.6\,\%$, lower left: B, $\bar{s} = 70.9\,\%$.

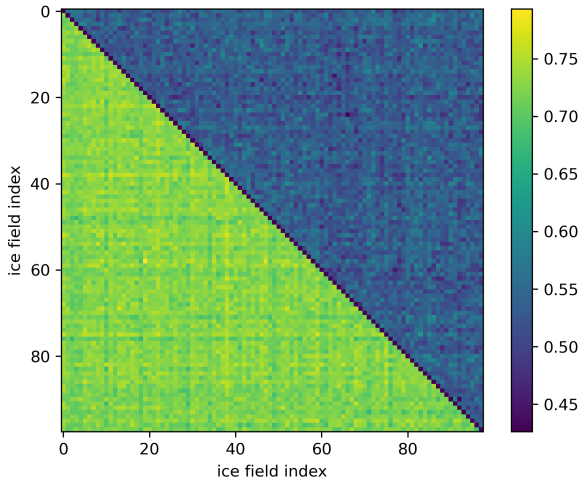

(b) upper right: C, $\bar{s} = 52.9\,\%$, lower left: D, $\bar{s} = 71.8\,\%$.

Figure 4: Cosine similarity of the generated ice floe fields for the four parameter sets in Table 1.

for the accuracy. If the floe field generation method presented above should be used to copy the real floe field by a synthetic one, the precision between all fields should be as close as possible. This would then conclude that all synthetic floe fields are an accurate representation of the real floe field. If, on the other hand, the synthetic floe fields should represent arbitrary areas of e.g. the marginal ice zone without the need of direct comparison to full scale data, the precision should be as wide as possible, to represent a wide range of possible floe field constellations.
The mean similarity values and the corresponding standard deviations are listed in Table 3. Figure 4 shows the cosine similarities for all four data sets graphically. The parameter sets A and B as well as C and D have the same diameter distribution, whereas the sets A and C as well as B and D have the same mean ice concentration. It can be seen that the influence of the actual diameter distribution is of a significant smaller influence on the similarity of the different ice fields than the ice concentration. This leads to the expected conclusion that the more ice floes in a given field, the higher the probability that two floes in two different fields are partly or fully overlapping.

DISCUSSION

Using the ice floe fields produced by the presented method as input to an icebreaking simulation,

a wide range of field setups can be covered. This is an advantage when a simulation should be applied on a general ice scenario of differently scattered ice floes, e.g. in the marginal ice zone. In this case, many ice fields can be created and used as simulation input into a Monte Carlo simulation, as done in (Sapp, 2023).
If, on the other hand, the simulation should be applied on one specific ice condition to compare the simulated data to full scale measurement data directly, the wide scattering of the different ice floe fields is a disadvantage and leads to significant deviations of the simulation results. In this case, the scattering should be reduced as much as possible. To obtain a more accurate ice field modelling, the ice condition observation must be improved. One option is to capture the size and position of every single floe. This can be done by visual airborne images, with a fixed camera at the ship as presented by Sandru et al. (2020) and Panchi et al. (2021) or by evaluating ice radar data. Based on more detailed ice observation data, the method proposed can be applied not only on circular shapes, but also on any other shape.
Another option is the optimization of observation-based ice documentation: Instead of documenting the whole ice field as once, it can be divided in several sub-fields. Every sub-field is then described separately and especially the ice concentration should be observed in higher detail. The latter option is described and evaluated in the following section.

Table 3: Statistical key parameters describing the similarity between different floe fields for each parameter set listed in Table 1.

Key	**Mean similarity**	**Standard deviation**
A	52.6%	5.95%
B	70.9%	7.36%
C	52.9%	5.94%
D	71.8%	7.45%

Improved model
Instead of one global ice field characteristics, the field is divided into multiple sub-fields with its own characteristics each. This respects local differences in the ice field such as channels of almost open water as well as more dense areas. As described above, the influence of the actual diameter distribution on the scattering is neglectable in comparison to the influence of the ice concentration. Therefore, only the concentration is varied in the different sub-fields whereas the diameter distribution is kept constant over the whole field. The field is divided into nine different zones arranged as a three times three grid. The diameter distribution is the same as in the parameter set D. The concentration values are

$$\begin{pmatrix} 80 & 85 & 80 \\ 45 & 50 & 50 \\ 85 & 80 & 75 \end{pmatrix} \tag{18}$$

with the mean ice concentration equal to the mean ice concentration of parameter set D. This new parameter set for the divided floe field is called D'.
The exact values for the mean similarity and the standard deviation are listed in Table 4. Comparing the multi-zone floe fields with the corresponding single-zone floe fields shows a minor improvement of the similarity and therefore the precision. Nevertheless, this improvement is below $1\,\%$ regarding the mean similarity value. Figure 5 shows all similarity values for both

Table 4: Statistical key parameters describing the similarity between the single-zone floe field with parameters D and the multi-zone floe field with specified concentration values.

Key	Mean similarity	Standard deviation
D	71.8%	7.45%
D'	72.4%	7.46%

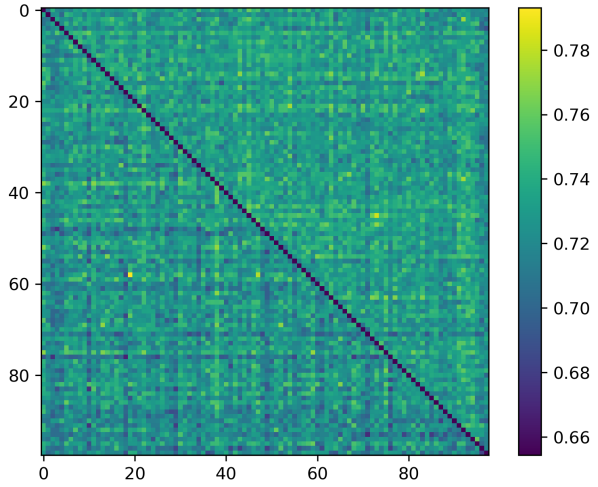

Figure 5: upper right: D', $\bar{s} = 72.4\,\%$, lower left: D, $\bar{s} = 71.8\,\%$

configurations. Since the improvement of the precision is as small, the ice observation of smaller grid cells is not worth the higher observation work.

CONCLUSION

The proposed method creates ice floe fields based on the ice observation parameters ice concentration, ice thickness and the diameter distribution within the floe field. The floes are placed randomly in a predefined area to match the given concentration and diameter distributions. This placement allows to create a huge variability of floe fields, which can then be used as input into a Monte-Carlo simulation. The proposed method is not able to represent one specific ice field pattern, but the general ice field characteristics. Therefore, using the floe fields generated by this method on full-scale data is limited to distribution comparisons (such as spectra) rather than direct measurement signal comparisons. For the latter, direct floe monitoring either by optical data or by radar observation is preferred.

REFERENCES

Agnieszka Herman. Molecular-dynamics simulation of clustering processes in sea-ice floes. *Physical Review E*, 84(5):056104, 2011.

Agnieszka Herman. Influence of ice concentration and floe-size distribution on cluster formation in sea-ice floes. *Central European Journal of Physics*, 10:715–722, 2012.

Mark A Hopkins, Susan Frankenstein, and Alan S Thorndike. Formation of an aggregate scale in arctic sea ice. *Journal of Geophysical Research: Oceans*, 109(C1), 2004.

Luofeng Huang, Bojan Igrec, and Giles Thomas. New tools to generate realistic ice floe fields for computational models. *Journal of Offshore Mechanics and Arctic Engineering*, 144(4): 044503, 06 2022.

Sveinung Løset. Discrete element modelling of a broken ice field—part ii: simulation of ice loads on a boom. *Cold regions science and technology*, 22(4):349–360, 1994.

Nabil Panchi, Ekaterina Kim, and Anirban Bhattacharyya. Supplementing remote sensing of ice: Deep learning-based image segmentation system for automatic detection and localization of sea-ice formations from close-range optical images. *IEEE Sensors Journal*, 21(16):18004–18019, 2021.

Andrei Sandru, Heikki Hyyti, Arto Visala, and Pentti Kujala. A complete process for shipborne sea-ice field analysis using machine vision. *IFAC-PapersOnLine*, 53(2):14539–14545, 2020.

Lina Sapp. Development of a floe-ice breaking simulation for the generation of propeller-ice load spectra. Master's thesis, Hamburg University of Technology, 2023.

Shanshan Sun and Hayley H Shen. Simulation of pancake ice load on a circular cylinder in a wave and current field. *Cold Regions Science and Technology*, 78:31–39, 2012.

Yaoyuan Zhang, Tongqiang Yu, Kun Liu, and Junji Xiang. Research on numerical generation of polar ice floe field based on surveying and mapping data. In *Fifth International Conference on Geology, Mapping, and Remote Sensing (ICGMRS 2024)*, volume 13223, pages 604–613. SPIE, 2024.

Z Zong, B Y Yang, Z Sun, and G Y Zhang. Experimental study of ship resistance in artificial ice floes. *Cold Regions Science and Technology*, page 103102, 2020.